HHS Public Access

Author manuscript

J Bone Miner Res. Author manuscript; available in PMC 2018 April 01.

Published in final edited form as:

J Bone Miner Res. 2017 April ; 32(4): 688–697. doi:10.1002/jbmr.3044.

Lactation-Induced Changes in the Volume of Osteocyte Lacunar-Canalicular Space Alter Mechanical Properties in Cortical Bone Tissue

Serra Kaya[1], **Jelena Basta-Pljakic**[1], **Zeynep Seref-Ferlengez**[1], **Robert J Majeska**[1], **Luis Cardoso**[1], **Timothy Bromage**[2], **Qihong Zhang**[3], **Carol R Flach**[3], **Richard Mendelsohn**[3], **Shoshana Yakar**[4], **Susannah P Fritton**[1], and **Mitchell B Schaffler**[1]

[1]Department of Biomedical Engineering, City College of New York, New York, NY, USA

[2]Department of Biomaterials, New York University College of Dentistry, New York, NY, USA

[3]Department of Chemistry, Rutgers University, Newark, NJ, USA

[4]Department of Basic Science, New York University College of Dentistry, New York, NY, USA

Abstract

Osteocytes can remove and remodel small amounts of their surrounding bone matrix through osteocytic osteolysis, which results in increased volume occupied by lacunar and canalicular space (LCS). It is well established that cortical bone stiffness and strength are strongly and inversely correlated with vascular porosity, but whether changes in LCS volume caused by osteocytic osteolysis are large enough to affect bone mechanical properties is not known. In the current studies we tested the hypotheses that (1) lactation and postlactation recovery in mice alter the elastic modulus of bone tissue, and (2) such local changes in mechanical properties are related predominantly to alterations in lacunar and canalicular volume rather than bone matrix composition. Mechanical testing was performed using microindentation to measure modulus in regions containing solely osteocytes and no vascular porosity. Lactation caused a significant (~13%) reduction in bone tissue-level elastic modulus ($p < 0.001$). After 1 week postweaning (recovery), bone modulus levels returned to control levels and did not change further after 4 weeks of recovery. LCS porosity tracked inversely with changes in cortical bone modulus. Lacunar and canalicular void space increased 7% and 15% with lactation, respectively ($p < 0.05$), then returned to control levels at 1 week after weaning. Neither bone mineralization (assessed by high-resolution backscattered scanning electron microscopy) nor mineral/matrix ratio or crystallinity (assessed by Raman microspectroscopy) changed with lactation. Thus, changes in bone mechanical properties induced by lactation and recovery appear to depend predominantly on changes in osteocyte LCS dimensions. Moreover, this study demonstrates that tissue-level cortical bone mechanical

Address correspondence to: Mitchell B Schaffler, PhD, Department of Biomedical Engineering, The City College of New York, 160 Convent Avenue, ST-401, New York, NY 10031, USA. mschaffler@ccny.cuny.edu.

Disclosures

All authors state that they have no conflicts of interest.

Authors' roles: SK and MBS and generated the hypothesis, conducted the experiments, data collection, analyses and writing, and are responsible for the integrity of the data. SY provided the mice used in these studies and intellectual input. ZS-F assisted with microindentation studies. JB-P and TB assisted with imaging and BSEM studies. RM, CRK, and QZ assisted with Raman microspectroscopy studies. LC, SPF, and RJM contributed intellectual input and writing.

properties are rapidly and reversibly modulated by osteocytes in response to physiological challenge. These data point to a hitherto unappreciated role for osteocytes in modulating and maintaining local bone mechanical properties.

Introduction

Osteocytes, which comprise some 90% to 95% of all adult bone cells,[1,2] have long been recognized as capable of modifying the extracellular matrix that surrounds them; however, the physiological and functional consequences of those modifications remain poorly understood. Evidence that osteocytes could alter local bone matrix structure dates from early histological observations of von Recklinghausen[3] and later ultrastructural investigations of Baud showing both rough and smooth regions along osteocyte lacunar walls.[4] Belanger,[5] in the 1960's, first introduced the term "osteocytic osteolysis" to describe the observation that osteocytes remodeled, and especially removed, bone from their lacunar wall. Since then osteocytic osteolysis has been demonstrated to occur in response to a variety of physiological challenges including microgravity, hibernation, PTH treatment, and lactation.[6–10] In particular, a number of recent studies have used lactation to explore the mechanism, extent, and reversibility of osteocytic osteolysis.[11,12] Expression by osteocytes of several enzymes associated with bone matrix catabolism including tartrate-resistant acid phosphatase (TRAP), carbonic anhydrase 2, matrix metalloproteinase (MMP)-10, and MMP-13, has also been demonstrated in physiological stress states where osteocytic osteolysis occurs, and these have been speculated to play a role in this localized bone removal.[9,13–15] Qing and colleagues[11] recently reported osteocyte expression of cathepsin K (CatK) during lactation-induced osteocytic osteolysis, suggesting an unexpected role for this so-called osteoclast protease in removing bone from lacunar and canalicular walls. Indeed recent studies by Lotinun and colleagues[16] confirmed that absence of CatK from the osteoblast/osteocyte lineage attenuates lactation-induced osteocytic osteolysis. Yet although osteocytic osteolysis occurs in a variety of physiological circumstances, its functional—and particularly mechanical—consequences for bone remain largely unknown.

It has long been appreciated that cortical bone modulus and strength are strongly and inversely dependent on the porosity of bone.[17–21] However, this interdependency has been explored principally in relation to large voids such as bone remodeling spaces and vascular pores (>30 μm diameter). Whether changes in the size of smaller but very widespread void spaces (eg, osteocyte lacunae and canaliculi) can similarly alter the local material/mechanical properties of bone is not known. Furthermore, osteocytic osteolysis has the potential to alter local bone matrix composition (eg, the ratio of bone mineral to the organic matrix), which could also alter the material properties of cortical bone. However, this possibility remains unexplored.

In the current study, we tested two hypotheses: (1) that the elastic modulus of bone changes at the tissue level in response to lactation and postlactation recovery in mice; and (2) that such local changes in mechanical properties are related predominantly to alterations in lacunar and canalicular volume.

Materials and Methods

Lactation model and experimental design

Female 11-week-old C57BL/6 mice were mated and randomly assigned to one of four groups (n = 5/group). Group 1 was euthanized immediately after parturition (Pregnancy, age = 14 weeks); group 2 was euthanized after 2 weeks of lactation (Lactation, age = 16 weeks); and the remaining mice (Groups 3 and 4) were force-weaned after 2 weeks of lactation. Group 3 mice were allowed to recover for 1 week after forced weaning (1W Recovery, age = 17 weeks) while group 4 mice recovered for 4 weeks (4W Recovery, age = 20 weeks), and then they were euthanized. For the Lactation and Recovery groups (Groups 2–4), litter size was fixed at three to five pups to normalize the lactation stress. Additional groups of age-matched nulliparous mice served as controls for 0, 2, and 4 weeks postparturition animals (n = 5/group). Mice were groups housed (4 to 5 mice per cage) and had access to normal rodent chow and water *ad libitum* throughout the study. Femurs were collected immediately after euthanasia at the time points indicated above; left femurs were frozen at −20°C prior to mechanical testing and right femurs were fixed in 10% neutral buffered formalin for 3 days and then transferred to 70% ethanol prior to processing for microarchitectural studies. All animal procedures were IACUC approved. All analyses were performed blinded to specimen experimental conditions.

Micromechanical analysis

Microindentation was used to test local changes in bone elastic modulus in pregnancy, lactation, and recovery. The small size of the indenter allowed us to sample multiple regions containing only bone matrix and the osteocyte lacunar canalicular space (LCS), and to avoid primary vascular canals and resorption spaces triggered by the lactation. However, microindentation was also preferable to nanoindentation in that each indented region mechanically sampled a large enough tissue region to include numerous canaliculi and at least one osteocyte on average. We previously showed that the nominal indent size in rodent bone under the test conditions used here is approximately 40 μm × 40 μm with depth of approximately 8 to 10 μm.[22] Frozen femur specimens for each group were thawed at room temperature before mechanical testing. Three transverse sections (1 mm thick) were cut from each mid-diaphysis using a diamond wafering saw. Sections were surface polished with graded carborundum paper and diamond paste to achieve a 0.25 μm finish and plano-parallel surfaces (tolerances for parallelism: <5 μm). Sections were kept hydrated with Ca^{2+}-supplemented PBS to reduce surface demineralization throughout sectioning, polishing, and mechanical testing.[23,24] Measurements were performed in the anterior (A) and posterior (P) quadrants of femoral cross-sections, where we could reliably perform five or more indent tests within each region. In addition, specimens were prepared and tested in a hydrated state, so indentation did not produce the microcracks around the indent residuals often reported in dried bone samples. Indents were separated by ~100 μm (greater than two indent widths) to avoid interactions with each other.[25] Medial and lateral cortices of the mouse femur could not be adequately sampled; the acute curvature of the medial cortex did not consistently allow the full number of well-positioned indent tests we required, whereas the lateral cortex often contained too many vascular canals to allow adequate sampling. Indents were performed using a Wilson microindenter equipped with a diamond Vickers microindenter tip

using 50*g* of applied force with a 10-s dwell time before unloading. All indents included in the final data set were symmetrical; ie, the major axis lengths were within 5% of each other. We had previously found that indents located directly over a vascular space were asymmetric and/or exhibited poorly defined edges, and consequently those indents were excluded from the final data set.[22] Elastic modulus (Ei) values were calculated from indentation hardness (Hv) values measured directly from individual indent profiles at magnification of ×400 (Fig. 1*A, B*), using the formula: Ei = 0.36Hv + 0.58 (R^2 = 93%).[22,26, 27]

Assessment of lacunar-canalicular void space

Backscattered scanning electron microscopy measurements of lacunar and canalicular area—Measurements of lacunar and canalicular areas were performed on images acquired by a scanning electron microscope equipped with a backscattered electron detector following a modification of the method of Qing and colleagues.[11] Backscattered scanning electron microscopy (BSEM) provides very high contrast images of void spaces versus bone matrix, and are easily thresholded for measurement. Lacunar measurements were made from the femoral bone cross-sections previously used for microindentation (Fig. 2*A*). Sections were prepared for BSEM by dehydration in graded ethanol and then transferred into hexamethyldisilazane for 15 min to remove ethanol. Samples were then dried overnight at 30°C, after which they were carbon coated. Images were acquired using field emission scanning electron microscopy (Zeiss EVO 50 SEM) operated in back-scattered mode at 15 kV accelerating voltage, 400 pA current, and 16 mm working distance. Images were thresholded using the Otsu's method in ImageJ (NIH, Bethesda, MD, USA; https://imagej.nih.gov/ij/) and areas were measured for all lacunae in the anterior quadrant of the femoral cortex. The entire anterior quadrant was examined to determine mean lacunar area (Ot.Lc.Ar, μm^2) and percent total lacunar porosity (% Lc.Ar = total lacunar area/ bone area × 100). Because canaliculi run parallel to the cross-sectional surface, there were too few canalicular profiles for reliable measurements. Instead, canaliculi were measured from longitudinal sections prepared from the adjacent diaphyseal cortical bone, immediately distal to the previous sample. Furthermore, canaliculi in the anterior cortex of mouse femurs are highly parallel in the radial direction, thus we used frontal sections through this cortex to allow visualization of large numbers of canaliculi in cross-sectional profile (Fig. 2*B*). Samples were embedded in PMMA, anterior diaphyseal surfaces were polished to mid-cortex using carborundum paper, fine polished, and carbon coated. High-magnification BSEM images of each field of view (60 nm pixel size) were acquired (discussed in detail in the proceeding section). Images were thresholded as described above. Mean area per canaliculus (Ca.Ar, μm^2) was determined from 10 randomly chosen 100-μm^2 fields were measured (~200 canaliculi per bone) and percent total canalicular porosity (% Ca.Ar = total canalicular area/ bone area × 100) determined using ImageJ.

Structured illumination microscopy measurements of lacunar and canalicular areas—We measured lacunar-canalicular changes using structured illumination microscopy (SIM), a novel fluorescence-based super-resolution microscopy approach that uses contrast enhancement techniques in combination with Fourier-based reconstruction to permit resolution on the order of 85 to 100 nm in the *x-y* plane.[28,29] For SIM imaging, formalin-fixed contralateral femora from lactation/recovery studies were cut in half at midshaft and

the proximal halves were stained en bloc with basic fuchsin in order to highlight the LCS. After staining, bones were embedded in poly(methyl methacrylate) (PMMA). Transverse sections were cut at the mid-shaft face of the block using a diamond wafering saw (Leica 1600 Sawing Microtome) and polished to a thickness of 90 μm using graded carborundum paper and diamond paste to achieve a final finish of 0.25 μm. Sections were then mounted on glass slides with high-precision coverslips. SIM images were obtained using a Zeiss Elyra S. 1 super-resolution microscope equipped with Zen software (Zeiss, Thornwood, NY). Sections were illuminated at 561 nm wavelength light and examined using a ×63 magnification oil-immersion objective (N.A. = 1.4 mm). Five grid rotations were used to maximize the image resolution. Laser power, exposure time, and gain were set at 6%, 100 msec, and 6, respectively. In preliminary studies we found that SIM imaging penetrates ~20 μm deep into fully mineralized bone before image quality becomes degraded; therefore, sampling sites were imaged to a depth of 20 μm, with Z-series images acquired at 0.126 μm intervals. Osteocytes were examined at multiple sampling sites within the anterior femoral cortex, which is the equivalent area to that tested mechanically in the contralateral femurs. Only lacunae that could be entirely visualized within a sampling region after 3D reconstruction were used for data collection (Fig. 2*C*), which assured that we examined only osteocyte voids and not small vessels. Typically, 10 to 12 lacunae per bone region met this completeness criterion. To avoid the potential *z*-axis elongation inherent in SIM and confocal 3D images,[30] measurements of lacunar area were made from single optical planes and averaged. Canalicular areas were measure from *z*-plane reconstructions that provided cross-sectional views of canaliculi. Areas were determined for a circular projection based on the small (*x*-axis) dimension of a given canaliculus to avoid the effects of *z*-axis elongation; approximately 150 canaliculi per bone were measured.

Compositional properties of cortical bone tissue

BSEM—High-resolution BSEM was used to test for changes in the bone matrix mineral content between adjacent canaliculi resulting from lactation and recovery. These studies were conducted on the same longitudinal sections images used for canalicular area measurements described above. This allowed visualization of large numbers of canaliculi in cross-sectional profile and measurement of the mineralization profiles between adjacent canaliculi using BSEM. The high magnification BSEM images (60 nm pixel size) were acquired sequentially with constant electron beam energy (15 kV) with approximately 60 nm beam diameter, 600 pA current, and 9 mm working distance. Using a Monte Carlo simulation, the penetration depth of the electron beam into bone for these scanning conditions is approximately 1 μm. Acquisition of the high-magnification images needed to measure bone matrix between canaliculi precluded the simultaneous inclusion of a phantom for absolute gray-level calibration in BSEM. Instead, high-resolution images were acquired in rapid sequence to minimize effects of voltage variations and an internal normalization approach was used to allow comparison of mineralization profiles of the bone between pairs of canaliculi, following recently reported by Nango and colleagues[31] to measure fine bone matrix mineralization properties from synchrotron X-ray microscopy. Histogram normalization using the Otsu method and mineralization measurements were performed in ImageJ. The 1% brightest and 1% darkest values were discarded from the histogram of each image and the rest of the histogram gray levels were linearly expanded in between 0 and 255

(black defined from lacunar or vascular spaces). Further enlarged images typically containing 10 to 15 canaliculi per field were used for measurement (Fig. 5*A*). These enlarged measurement fields were taken from bone regions that were located within ~8 μm of the lacunar margin; in pilot studies we found that this distance represents about half the mean distance between adjacent osteocyte lacunae in the region of the mouse femoral cortex examined. Canaliculi within a measurement field were identified and the gray level profile of the bone matrix was then measured radially from a canalicular edge at 80 nm increments until half the distance to an adjacent canalicular edge was reached. Because we used longitudinal sections to visualize canaliculi in cross-sections, there was no underlying void space in the sampling volume between two canaliculi. Therefore, gray-level versus distance curves were used to compare mineral content distribution in matrix between canaliculi among experimental groups.

Raman microspectroscopy—BSEM measurements provided critical information about how the relative mineral distributions between canaliculi changes with lactation and recovery. However, given the inherent calibration limitation for these high-magnification BSEM images, we used Raman microspectroscopy as a complementary approach to determine mineral content and composition of the bone matrix during lactation and recovery. Raman studies examined the same mid-diaphyseal cross-sections and regions used for SIM imaging. Raman spectra were collected using a WITecAlpha-300R Plus confocal Raman microscope (Ulm, Germany). The semiconductor diode excitation laser was operated in the near infrared range (785 nm) with a 0.5-μm-diameter spot size. This spot size was small enough to avoid including osteocyte lacunae visible on the bone surface in the measurements, allowing us to capture Raman spectra in interlacunar bone areas that contained only matrix and canaliculi. Spectra were sampled using a ×100 magnification oil immersion objective (N.A. = 1.25). Raman spectra ($n = 20$) were captured from the anterior quadrant of each femur cross-section, examined and averaged per bone. Each spectrum was acquired at the mid-cortex width at 20 μm distance from each other. Data acquisition and analysis were performed using WITec Project Plus 4.1 software and a custom Matlab code. Spectra were normalized with respect to strongest phosphate band area using Matlab. The following parameters were determined as described by Michael D Morris and his colleagues (Wallace and colleagues,[32] Tarnowski and colleagues,[33] Gamsjaeger and colleagues,[34] Gong and colleagues,[35] Timlin and colleagues,[36] and McCreadie and colleagues[37]): (1) mineral/matrix ratio, which measures of the degree of mineralization of the tissue; (2) carbonate/phosphate ratio, which is an indication of carbonate substitution for phosphate in crystal lattice; and (3) mineral crystallinity, an indicator of mineral crystal size and/or lattice perfection. Measurements of individual spectra were made using a custom-written Matlab code. Three band areas were determined: phosphate band (960 cm^{-1}), carbonate band (1070 cm^{-1}), and Amide I band (1620 to 1700 cm^{-1}). Mineral/matrix ratios were obtained by dividing the integrated band areas of phosphate to amide I. Carbonate/phosphate ratios were calculated by dividing carbonate band areas by phosphate band areas. Mineral crystallinity information was determined by taking the inverse of full-width at half-maximum (FWHM) for the phosphate band (crystallinity = 1/FWHM).

Statistical analysis

All data are reported as mean ± SD. IBM SPSS statistics software was used to perform statistical analyses as indicated for individual experiments. Differences in elastic modulus, lacunar and canalicular area and porosity, mineral/matrix ratio, carbonate/phosphate ratio, and crystallinity index among groups were tested with a one-way ANOVA test and post hoc comparisons were performed with Fisher's least significant difference (LSD) with corrections applied to account for differences in group sizes.

Results

Micromechanical changes in pregnancy-lactation-recovery

Pregnancy had no effect on the local bone elastic modulus of femoral bone as measured using microindentation. Modulus values of anterior cortices were 21.2 ± 1.2 GPa and 21.3 ± 0.9 GPa in mice at parturition and in age-matched nulliparous controls, respectively. Posterior cortical modulus values were 20.2 ± 0.6 GPa and 20.4 ± 0.7 GPa, at parturition and in age-matched nulliparous controls, respectively.

In contrast, lactation caused marked reductions in bone elastic modulus (10% and 13% at posterior and anterior locations, respectively, $p < 0.001$; Fig. 3*A, B*). Examination of cortical bone cross-sections at the mid-diaphysis showed no evidence of intracortical resorption in either control or lactation groups. Thus, changes in tissue modulus must be coupled to changes at the osteocyte and/or bone matrix level. By 1 week after lactation (1W Recovery), the reduced modulus values had returned to age-matched control levels and did not increase further even after 4 weeks post-lactation (4W Recovery). No differences in bone elastic modulus were seen among the nulliparous control groups (Fig. 3).

Because no further changes were found in elastic modulus after 1 week of recovery after lactation, all detailed analyses of lacunar and canalicular space and bone matrix composition (described below) were performed on bones from the Control (age-matched nulliparous mice for 2 weeks postparturition), Lactation, and 1W Recovery groups.

Microstructural changes in osteocyte lacunar-canalicular void space during lactation and recovery

In control cortical bone, BSEM-based average lacunar and canalicular areas were 17.3 ± 1.2 μm^2 and 0.13 ± 0.012 μm^2, respectively (Fig. 4*A, B*). The corresponding lacunar void volume fraction was approximately 0.8% (Fig. 4*C*). However, because of the large number of canaliculi, the overall canalicular void fraction was approximately 2.8% (Fig. 4*C*). With lactation, lacunar and canalicular areas increased by 7% and 15%, respectively, resulting in overall lacunar and canalicular porosities of ~1% and ~3.5%, respectively ($p < 0.05$ versus control for each; Fig. 4). Increased lacunar and canalicular area and porosity values returned to control levels by 1W Recovery (Fig. 4). As found in BSEM-based measurements, SIM images showed similar lacunar and canalicular area and porosity increases with lactation and decreases to control levels by 1W Recovery. SIM-derived lacunar areas were similar to BSEM measured areas in all experimental groups, although the SIM-derived values in the

lactation groups showed greater variability. On the other hand, the SIM-derived canalicular areas were 20% lower than BSEM values.

Bone tissue composition

Mineral content measured in BSEM images was lowest at canalicular walls, then increased rapidly and exponentially over the course of ~250 nm, becoming asymptotic as it approached the midpoint between adjacent canaliculi (Fig. 5*B*). Examination of multiple canalicular pairs showed that mineral content distribution was symmetric about the midpoint. Furthermore, even though canaliculi expanded in diameter during lactation, the BSEM-based mineral distribution between canalicular walls was unchanged from control bones (Fig. 5*B*). Raman spectroscopy revealed no differences in mineral to matrix ratio and in crystallinity among the lactation, 1-week recovery, and control groups ($p > 0.7$; Fig. 6*A, B*). However, lactation caused a reduction in the carbonate/phosphate ratio of approximately 30% ($p < 0.05$) that was not significantly changed following a 1-week recovery period (Fig. 6*C*).

Discussion

The results of this study demonstrate that the physiological demands of lactation are sufficient to cause changes in the local mechanical behavior of cortical bone—specifically a reduction of roughly 13% in elastic modulus. This local change in tissue modulus occurs in the absence of intracortical remodeling and is associated with a comparable expansion of the lacunar-canalicular space, consistent with an osteocyte-mediated process (osteocytic osteolysis). Changes in both elastic modulus and lacunar-canalicular dimensions were rapidly reversed once lactation ceased, returning to control levels within 1 week. Finally, assessment of matrix composition by BSEM and Raman spectroscopy indicated that the overall mineralization was not changed as a result of lactation and recovery. Consequently, the changes in mechanical properties were likely due principally to cumulative increases in void volume contributed by lacunae and canaliculi.

Previous lactation studies in rats and mice have shown changes in whole-bone mechanical properties that were explained on the basis of whole-bone geometry changes. Specifically, lactation caused marked reduction in whole-bone stiffness, which was attributed primarily to endocortical bone loss and cortical thinning.[38–40] However, recent computational analyses by Liu and colleagues[41] revealed that decreases in whole-bone stiffness with lactation are greater than those predicted from changes in diaphyseal geometry alone. This suggests that the bone material itself is altered by lactation. Our data support this prediction. Microindentation allowed assessment of elastic modulus in small regions (~40 μm square) independent of whole-bone geometry, and in tissue areas where no vascular porosities, with size similar to the indenter tip, were present. Thus, changes in modulus that we observed during lactation and recovery reflect only the small amount of bone matrix immediately beneath the microindenter. Furthermore, our modulus values are comparable to those reported in nanoindentation studies, 26 to 30 GPa.[42–44]

It is well established that elastic modulus of bone is highly dependent on large scale porosity (ie, vascular and remodeling spaces, 1% to 5% in mice).[17–21,45–48] However, the findings

of the current study indicate that changes at the much smaller length scale of the lacunar-canalicular level porosity can significantly influence bone mechanical properties. The overall lacunar-canalicular porosity in human, dog, rat, and mouse models has been reported in the range of 1% to 14% of total cortical bone volume, depending on the imaging techniques utilized.[45,49–53] The current studies show lacunar and canalicular porosities of approximately 1% and 2.5%, respectively, consistent with previous reports. Interestingly, the large numbers of canaliculi make their aggregate porosity space some 2.5-fold higher than the lacunar porosity. This is much larger than generally appreciated, but recently Benalla and colleagues[52] also found higher canalicular porosity than lacunar porosity in human bone. The osteocyte level void volume (~3.5% of cortical bone volume for both lacunae and canaliculi combined) places the LCS porosity into the same range as the vascular porosity.[45,48,49]

Although LCS and vascular porosities are of similar magnitude, they exhibit markedly different remodeling dynamics. Changes in vascular porosity are produced via osteoclastic bone remodeling and occur over months, whereas our studies show that alterations in the LCS void volume, with its concomitant changes in tissue mechanical properties, occurred over days to weeks. Thus, osteocyte regulation of LCS-level microporosity appears to be a key, rapid regulator of bone modulus in response to physiological stresses.

In the current studies, we used BSEM for measurements of lacunae and canaliculi. In addition, this study for the first time applied a super-resolution microscopy technique—SIM—to examine osteocytes and the LCS in situ. SIM is a fluorescence-based approach that is well suited for use on thick bone sections. In combination with basic fuchsin-stained undecalcified samples, SIM allowed visualization of osteocytes within lacunae, the pericellular space around the cell body, lacunae, and canaliculi, up to a depth of about 20 μm into cortical bone. Confocal microscopy also permits 3D imaging beyond the conventional limit both in lateral and axial dimensions,[54] but SIM has higher effective lateral resolution than confocal microscopy.[55] Although lacunar areas measured with BSEM and SIM had similar results, canalicular area values were lower in SIM measurements than BSEM. The reason for these discrepancies is not yet clear, but it seems likely that stain penetration into the bone matrix, which could vary depending on location (lacunae versus canaliculi) or LCS surface state (resting versus lactating) is a contributing factor. Differences between stain volume versus actual matrix volume is likely to contribute. Yet regardless of the imaging method used, the relative changes in LCS void space with lactation and recovery were similar to those found using BSEM.[11]

It was not clear whether osteocytic osteolysis could, in addition to altering LCS volume, cause compositional changes in the bone matrix. Alterations in bone matrix composition, mineralization in particular, have been shown to affect bone modulus.[56] Our quantitative BSEM studies on bone after lactation found no alterations in either the distribution or the amount of mineral in bone matrix located between canaliculi. In other words, bone is lost in a small region of bone immediately surrounding osteocytes and their processes (~60 to 80 nm radial width), beyond which the mineralization profile between the canalicular walls appears the same in lactating and control mice. The observations agree with recent data reported for human and mouse bone.[31,57,58] Raman microspectroscopy studies further

revealed that there were no differences in mineral/matrix ratio and crystallinity in the matrix between lactation and control bones, confirming that overall matrix mineralization was unchanged. Our Raman results were similar those reported by Wallace and colleagues.[32] It has long been proposed that the mineral immediately surrounding osteocytes is different from the more mature, larger apatite crystals away from the osteocytes. Calcium and phosphates along the LCS walls appear to be more labile and readily exchanged with the bone fluid.[59] Nango and colleagues[31] recently confirmed the existence of a small zone of mineral on canalicular walls that is rapidly mobilized in lactation and other stress states. Together, these data indicate that there are no changes in the overall mineral content of bone matrix after lactation in mouse, and so bulk changes in mineralization do not contribute to the changes in bone tissue material properties seen with lactation and recovery.

Our Raman microspectroscopy studies revealed a small decrease in carbonate/phosphate ratio in lactation compared to control bone that did not return to control levels with recovery from lactation during the short period we examined. Carbonate bonds in bone mineral are weaker than phosphate bonds[60] and thus carbonate moieties are more soluble than phosphates; accordingly, carbonate substituted hydroxyapatite has been referred to as a labile fraction of bone mineral.[60,61] Thus, it seems reasonable to speculate that carbonate loss is the major driver of the altered carbonate/phosphate ratio observed with lactation. Why carbonate levels do not recover upon remineralization remains unknown. From the standpoint of tissue level mechanical properties, previous Raman and Fourier transform-infrared (FTIR) studies by Donnelly and colleagues[56] and Miller and colleagues,[43] respectively, reported that carbonate/phosphate ratio in hydroxyapatite was not significant determinant for the bone tissue modulus. They found that changing carbonate/phosphate ratio did not influence bone tissue modulus. Thus it seems reasonable to conclude that the small changes in carbonate/phosphate ratio resulting from lactation do not influence bone tissue-level mechanical properties.

There is considerable evidence that osteocytes modify their perilacunar and pericanalicular matrix during reproductive cycles reviewed by Wysolmerski,[12,62] but the precise mechanisms of osteocytic osteolysis remain incompletely understood. The need to release mineral, rather than matrix constituents, from bone has long been considered the primary driver of osteocytic osteolysis,[6,8,10,31,53,63–67] and presumably such rapid mineral removal occurs through acidification of the fluid in the LCS. Data to support LCS acidification during lactation are lacking, but the ability of osteocytes to acidify their local microenvironment was recently demonstrated in sciatic neurectomy.[68] Interestingly, Qing and colleagues[11] reported an increase in CatK expression and several MMPs by osteocytes during lactation, suggesting that degradation of organic matrix occurs around osteocytes. Furthermore, TRAP, carbonic anhydrase 2, MMP-10, and MMP-13 expression by osteocytes have also been reported in response to lactation and other stressors (microgravity, sclerostin modulation).[9,13,14] Recently, Lotinun and colleagues[16] found that deletion of CatK from osteocytes markedly reduced lacunar enlargement during lactation, pointing to a dominant role for CatK in osteocytic osteolysis. The requirement for CatK for lacunar expansion implicates lysosomal involvement (and likely degradation of organic matrix constituents) in this aspect of osteocytic osteolysis. However, CatK seems less likely to participate in local remodeling of matrix around osteocyte processes. There is little available space to

accommodate lysosomes inside the osteocyte processes, except in regions closest to the cell body; furthermore, CatK is too large to move easily through the proteoglycan-containing extracellular space surrounding canaliculi.[69,70] As a result, loss of bone mineral in canalicular regions may result more from acidification rather than via simultaneous dissolution of mineral and breakdown of matrix, such as happens during osteoclastic resorption. Consistent with this idea, Sharma and colleagues[53] recently found that ovariectomy resulted principally in loss of mineral from canalicular walls. However, establishing the precise mechanism for canalicular enlargement requires further investigation.

In summary, our data indicate that osteocytic osteolysis during lactation results in a small increase in the osteocyte lacunar-canalicular space without altering the matrix mineral content. This rapid and reversible change appears to be the principal factor responsible for the decreased tissue modulus seen in lactation and its recovery when lactation ceases. Osteocyte-level changes in bone material properties have been shown in pathological circumstances, eg, high-dose glucocorticoids,[71] and osteocyte-targeted knockout of gap junctions.[72] However, the current studies are the first to our knowledge to show that changes at the osteocyte level during a physiological process can significantly, rapidly, and dynamically influence bone tissue level properties. These findings point to a hitherto unappreciated role for osteocytes in modulating and maintaining local bone mechanical properties.

Acknowledgments

This work was supported by grants AR041210 and AR057139 (to MBS) from the National Institute of Arthritis and Musculoskeletal and Skin Diseases, DK100246 (to SY) from the National Institute of Diabetes and Digestive and Kidney Diseases, SC1 DK103362 (to LC) from the National Institutes of Health; and 1333560 (to LC) from National Science Foundation. The content is solely the responsibility of the authors and does not necessarily represent the official views of the National Institutes of Health. SK received partial support from a doctoral fellowship from the Grove School of Engineering at the City College of New York. The Raman microscope was purchased through the State of New Jersey "ELF III Project 047-04 Polymer and Nanomaterials Characterization Facility" grant to the Rutgers-Newark Chemistry Department. We thank Prof. Jackie Li of CCNY Mechanical Engineering Department for use of microindenter, Damien Laudier for assistance with tissue preparation, Jessica Thomas for assistance with SIM analysis, Dr. Paolo E. Palacio-Mancheno for guidance with BSEM assessment.

References

1. Bonewald LF. The amazing osteocyte. J Bone Miner Res. 2011; 26(2):229–238. [PubMed: 21254230]
2. Schaffler MB, Kennedy OD. Osteocyte signaling in bone. Curr Osteoporos Rep. 2012; 10(2):118–125. [PubMed: 22552701]
3. von Recklinghausen, F. [Disorders over rachitis and osteomalacia] Untersurchungen uber rachitis and osteomalacia. Jena, Germany: Gustav Fischer Publisher; 1910. German
4. Baud CA. Morphology and inframicroscopic structure of osteocytes. Acta Anat. 1962; 51:209–225. [PubMed: 13966889]
5. Belanger LF. Osteocytic osteolysis. Calcif Tissue Res. 1969; 4(1):1–12. [PubMed: 4310125]
6. Steinberg B, Singh IJ, Mitchell OG. The effects of cold-stress. Hibernation, and prolonged inactivity on bone dynamics in the golden hamster, *Mesocricetus auratus*. J Morphol. 1981; 167(1):43–51. [PubMed: 7241597]

7. McGee-Lawrence ME, Carey HV, Donahue SW. Mammalian hibernation as a model of disuse osteoporosis: the effects of physical inactivity on bone metabolism, structure, and strength. Am J Physiol Regul Integr Comp Physiol. 2008; 295(6):R1999–R2014. [PubMed: 18843088]
8. Krempien B, Ritz E. Effects of parathyroid hormone on osteocytes. Ultrastructural evidence for anisotropic osteolysis and involvement of the cytoskeleton. Metab Bone Dis Relat Res. 1978; 1(1): 55–65.
9. Blaber EA, Dvorochkin N, Lee C, et al. Microgravity induces pelvic bone loss through osteoclastic activity, osteocytic osteolysis, and osteoblastic cell cycle inhibition by CDKN1a/p21. PLoS One. 2013; 8(4):e61372. [PubMed: 23637819]
10. Teti A, Zallone A. Do osteocytes contribute to bone mineral homeostasis? Osteocytic osteolysis revisited. Bone. 2009; 44(1):11–16. [PubMed: 18977320]
11. Qing H, Ardeshirpour L, Divieti Pajevic P, et al. Demonstration of osteocytic perilacunar/canalicular remodeling in mice during lactation. J Bone Miner Res. 2012; 27(5):1018–1029. [PubMed: 22308018]
12. Wysolmerski JJ. Osteocytes remove and replace perilacunar mineral during reproductive cycles. Bone. 2013; 54(2):230–236. [PubMed: 23352996]
13. Tang SY, Herber R-P, Ho SP, Alliston T. Matrix metalloproteinase-13 is required for osteocytic perilacunar remodeling and maintains bone fracture resistance. J Bone Miner Res. 2012; 27(9): 1936–1950. [PubMed: 22549931]
14. Kogawa M, Wijenayaka AR, Ormsby RT, et al. Sclerostin regulates release of bone mineral by osteocytes by induction of carbonic anhydrase 2. J Bone Miner Res. 2013 Dec; 28(12):2436–2448. [PubMed: 23737439]
15. Lloyd SA, Loiselle AE, Zhang Y, Donahue HJ. Evidence for the role of connexin 43-mediated intercellular communication in the process of intracortical bone resorption via osteocytic osteolysis. BMC Musculoskelet Disord. 2014; 15(1):122. [PubMed: 24716486]
16. Lotinun S, Kiviranta R, Carpentier V, et al. Osteocyte-specific deletion of cathepsin K prevents increased bone turnover, bone loss and bone fragility during lactation in mice. J Bone Miner Res. 2015; 30(Suppl 1)
17. Currey JD. The effect of porosity and mineral content on the Young's modulus of elasticity of compact bone. J Biomech. 1988; 21(2):131–139. [PubMed: 3350827]
18. Hernandez CJ, Beaupre GS, Keller TS, Carter DR. The influence of bone volume fraction and ash fraction on bone strength and modulus. Bone. 2001; 29(1):74–78. [PubMed: 11472894]
19. McCalden RW, McGeough JA, Barker MB, Court-Brown CM. Age-related changes in the tensile properties of cortical bone. The relative importance of changes in porosity, mineralization, and microstructure. J Bone Jt Surg Am. 1993; 75(8):1193–1205.
20. Dong XN, Guo XE. The dependence of transversely isotropic elasticity of human femoral cortical bone on porosity. J Biomech. 2004; 37(8):1281–1287. [PubMed: 15212934]
21. Currey J. Incompatible mechanical properties in compact bone. J Theor Biol. 2004; 231(4):569–580. [PubMed: 15488534]
22. Seref-Ferlengez Z, Basta-Pljakic J, Kennedy OD, Philemon CJ, Schaffler MB. Structural and mechanical repair of diffuse damage in cortical bone in vivo. J Bone Miner Res. 2014; 29(12): 2537. [PubMed: 25042459]
23. Boyce TM, Fyhrie DP, Glotkowski MC, Radin EL, Schaffler MB. Damage type and strain mode associations in human compact bone bending fatigue. J Orthop Res. 1998; 16(3):322–329. [PubMed: 9671927]
24. Gustafson MB, Martin RB, Gibson V, et al. Calcium buffering is required to maintain bone stiffness in saline solution. J Biomech. 1996; 29(9):1191–1194. [PubMed: 8872276]
25. Kruzic JJ, Kim DK, Koester KJ, Ritchie RO. Indentation techniques for evaluating the fracture toughness of biomaterials and hard tissues. J Mech Behav Biomed Mater. 2009; 2(4):384–395. [PubMed: 19627845]
26. Currey JD, Brear K. Hardness, Young's modulus and yield stress in mammalian mineralized tissues. J Mater Sci Mater Med. 1990; 1(1):14–20.

27. Rapoff AJ, Rinaldi RG, Hotzman JL, Daegling DJ. Elastic modulus variation in mandibular bone: a microindentation study of *Macaca fascicularis*. Am J Phys Anthropol. 2008 Jan; 135(1):100–109. [PubMed: 18058791]
28. Gustafsson MGL, Shao L, Carlton PM, et al. Three-dimensional resolution doubling in wide-field fluorescence microscopy by structured illumination. Biophys J. 2008; 94(12):4957–4970. [PubMed: 18326650]
29. Gustafsson MGL, Agard DA, Sedat JW. Doubling the lateral resolution of wide-field fluorescence microscopy using structured illumination. Proc SPIE. 2000; 3919:141–150. [Presented at: Three-Dimensional and Multidimensional Microscopy: Image Acquisition Processing VII, 141 (May 2, 2000)]. DOI: 10.1117/12.384189.
30. Lee GS, Miele LF, Turhan A, et al. Spatial calibration of structured illumination fluorescence microscopy using capillary tissue phantoms. Microsc Res Tech. 2009; 72(2):85–92. [PubMed: 18937249]
31. Nango N, Kubota S, Hasegawa T, Yashiro W, Momose A, Matsuo K. Osteocyte-directed bone demineralization along canaliculi. Bone. 2015; 84:279–288. [PubMed: 26709236]
32. Wallace JM, Golcuk K, Morris MD, Kohn DH. Inbred strain-specific effects of exercise in wild type and biglycan deficient mice. Ann Biomed Eng. 2010; 38(4):1607–1617. [PubMed: 20033775]
33. Tarnowski CP, Ignelzi MA, Morris MD. Mineralization of developing mouse calvaria as revealed by Raman microspectroscopy. J Bone Miner Res. 2002; 17(6):1118–1126. [PubMed: 12054168]
34. Gamsjaeger S, Masic A, Roschger P, et al. Cortical bone composition and orientation as a function of animal and tissue age in mice by Raman spectroscopy. Bone. 2010; 47(2):392–399. [PubMed: 20450992]
35. Gong B, Oest ME, Mann KA, Damron TA, Morris MD. Raman spectroscopy demonstrates prolonged alteration of bone chemical composition following extremity localized irradiation. Bone. 2013; 57(1):252–258. [PubMed: 23978492]
36. Timlin JA, Carden A, Morris MD, Rajachar RM, Kohn DH. Raman spectroscopic imaging markers for fatigue-related microdamage in bovine bone. Anal Chem. 2000; 72(10):2229–2236. [PubMed: 10845368]
37. McCreadie BR, Morris MD, Chen TC, et al. Bone tissue compositional differences in women with and without osteoporotic fracture. Bone. 2006; 39(6):1190–1195. [PubMed: 16901772]
38. Redd EH, Miller SC, Jee WSS. Changes in endochondral bone elongation rates during pregnancy and lactation in rats. Calcif Tissue Int. 1984; 36(1):697–701. [PubMed: 6442205]
39. Vajda EG, Bowman BM, Miller SC. Cancellous and cortical bone mechanical properties and tissue dynamics during pregnancy, lactation, and postlactation in the rat. Biol Reprod. 2001; 65(3):689–695. [PubMed: 11514329]
40. Miller SC, Bowman BM. Rapid improvements in cortical bone dynamics and structure after lactation in established breeder rats. Anat Rec A Discov Mol Cell Evol Biol. 2004; 276(2):143–149. [PubMed: 14752853]
41. Liu XS, Ardeshirpour L, VanHouten JN, Shane E, Wysolmerski JJ. Site-specific changes in bone microarchitecture, mineralization, and stiffness during lactation and after weaning in mice. J Bone Miner Res. 2012; 27(4):865–875. [PubMed: 22189918]
42. Akhter MP, Fan Z, Rho JY. Bone intrinsic material properties in three inbred mouse strains. Calcif Tissue Int. 2004; 75(5):416–420. [PubMed: 15592798]
43. Miller LM, Little W, Schirmer A, Sheik F, Busa B, Judex S. Accretion of bone quantity and quality in the developing mouse skeleton. J Bone Miner Res. 2007; 22(7):1037–1045. [PubMed: 17402847]
44. Jiao Y, Chiu H, Fan Z, et al. Quantitative trait loci that determine mouse tibial nanoindentation properties in an F2 population derived from C57BL/6J X C3H/HeJ. Calcif Tissue Int. 2007; 80(6):383–390. [PubMed: 17551771]
45. Cardoso L, Fritton SP, Gailani G, Benalla M, Cowin SC. Advances in assessment of bone porosity, permeability and interstitial fluid flow. J Biomech. 2013; 46(2):253–265. [PubMed: 23174418]
46. Carter DR, Hayes WC. The compressive behavior of bone as a two-phase porous structure. J Bone Joint Surg Am. 1977; 59(7):954–962. [PubMed: 561786]

47. Martin RB, Ishida J. The relative effects of collagen fiber orientation, porosity, density, and mineralization on bone strength. J Biomech. 1989; 22(5):419–426. [PubMed: 2777816]
48. Schaffler MB, Burr DB. Stiffness of compact bone: effects of porosity and density. J Biomech. 1988; 21(1):13–16. [PubMed: 3339022]
49. Cowin SC. Bone poroelasticity. J Biomech. 1999; 32(3):217–238. [PubMed: 10093022]
50. Schneider P, Stauber M, Voide R, Stampanoni M, Donahue LR, Müller R. Ultrastructural properties in cortical bone vary greatly in two inbred strains of mice as assessed by synchrotron light based micro- and nano-CT. J Bone Miner Res. 2007; 22(10):1557–1570. [PubMed: 17605631]
51. Schneider P, Meier M, Wepf R, Müller R. Serial FIB/SEM imaging for quantitative 3D assessment of the osteocyte lacuno-canalicular network. Bone. 2011; 49(2):304–311. [PubMed: 21514408]
52. Benalla M, Palacio-Mancheno PE, Fritton SP, Cardoso L, Cowin SC. Dynamic permeability of the lacunar-canalicular system in human cortical bone. Biomech Model Mechanobiol. 2014; 13(4): 801–812. [PubMed: 24146291]
53. Sharma D, Ciani C, Marin PA, Levy JD, Doty SB, Fritton SP. Alterations in the osteocyte lacunar-canalicular microenvironment due to estrogen deficiency. Bone. 2012; 51(3):488–497. [PubMed: 22634177]
54. Pawley, JB. Handbook of biological confocal microscopy. Boston, MA: Springer US; 2006. Fundamental limits in confocal microscopy; p. 20-42.
55. Gustafson MGL. Surpassing the lateral resolution limit by a factor of two using structured illumination microscopy. J Microsc. 2000; 198:82–87. [PubMed: 10810003]
56. Donnelly E, Boskey AL, Baker SP, van der Meulen MCH. Effects of tissue age on bone tissue material composition and nanomechanical properties in the rat cortex. J Biomed Mater Res A. 2010; 92(3):1048–1056. [PubMed: 19301272]
57. Hesse B, Varga P, Langer M, et al. Canalicular network morphology is the major determinant of the spatial distribution of mass density in human bone tissue - evidence by means of synchrotron radiation phase-contrast nano-CT. J Bone Miner Res. 2014; 30(2):346–356.
58. Kerschnitzki M, Kollmannsberger P, Burghammer M, et al. Architecture of the osteocyte network correlates with bone material quality. J Bone Miner Res. 2013; 28(8):1837–1845. [PubMed: 23494896]
59. Gardinier JD, Al-Omaishi S, Morris MD, Kohn DH. PTH signaling mediates perilacunar remodeling during exercise. Matrix Biol. 2016; 52–54:162–175.
60. Elliott JC. Calcium phosphate biominerals. Reviews in Mineralogy and Geochemistry. 2002; 48(1): 427–453.
61. Wopenka B, Pasteris JD. A mineralogical perspective on the apatite in bone. Mater Sci Eng C. 2005; 25(2):131–143.
62. Wysolmerski JJ. Osteocytic osteolysis: time for a second look? Bonekey Rep. 2012; 1:229. [PubMed: 24363929]
63. Mosekilde L, Melsen F. A tetracycline-based histomorphometric evaluation of bone resorption and bone turnover in hyperthyroidism and hyperparathyroidism. Acta Med Scand. 1978; 204:97–102. [PubMed: 685737]
64. Bonucci E, Gherardi G. Osteocyte ultrastructure in renal osteodystrophy. Virchows Arch A Pathol Anat Histol. 1977; 373(3):213–231. [PubMed: 140505]
65. Bonucci E, Gherardi G, Faraggiana T. Bone changes in hemodialyzed uremic subjects. Comparative light and electron microscope investigations. Virchows Arch A Pathol Anat Histol. 1976; 371(3):183–198. [PubMed: 823694]
66. Krempien B, Manegold C, Ritz E, Bommer J. The influence of immobilization on osteocyte morphology. Virchows Arch A Pathol Anat Histol. 1976; 370(1):55–68. [PubMed: 818789]
67. Atkins GJ, Findlay DM. Osteocyte regulation of bone mineral: a little give and take. Osteoporos Int. 2012; 23(8):2067–2079. [PubMed: 22302104]
68. Sano H, Kikuta J, Furuya M, Kondo N, Endo N, Ishii M. Intravital bone imaging by two-photon excitation microscopy to identify osteocytic osteolysis in vivo. Bone. 2015; 74:134–139. [PubMed: 25624000]

69. Wang L, Wang Y, Han Y, et al. In situ measurement of solute transport in the bone lacunar-canalicular system. Proc Natl Acad Sci U S A. 2005; 102(33):11911–11916. [PubMed: 16087872]

70. Fritton SP, Weinbaum S. Fluid and solute transport in bone: flow-induced mechanotransduction. Annu Rev Fluid Mech. 2009; 41:347–374. [PubMed: 20072666]

71. Lane NE, Yao W, Balooch M, et al. Glucocorticoid-treated mice have localized changes in trabecular bone material properties and osteocyte lacunar size that are not observed in placebo-treated or estrogen-deficient mice. J Bone Miner Res. 2006; 21(3):466–476. [PubMed: 16491295]

72. Bivi N, Nelson MT, Faillace ME, Li J, Miller LM, Plotkin LI. Deletion of Cx43 from osteocytes results in defective bone material properties but does not decrease extrinsic strength in cortical bone. Calcif Tissue Int. 2012; 91(3):215–224. [PubMed: 22865265]

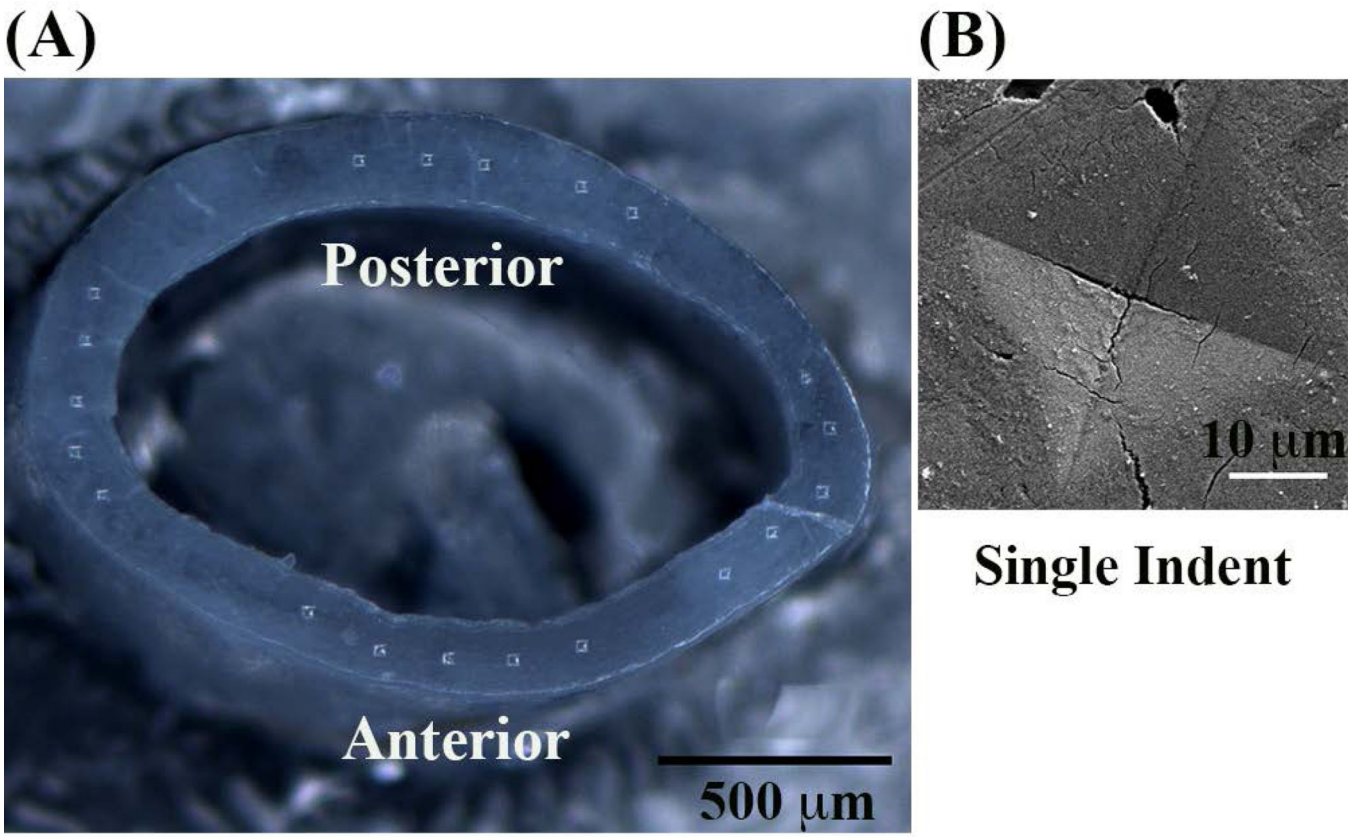

Fig. 1.

(*A*) Mouse femoral mid-diaphysis cross-section showing position of microindents and (*B*) enlarged scanning electron microscopy image shows a single residual indent profile.

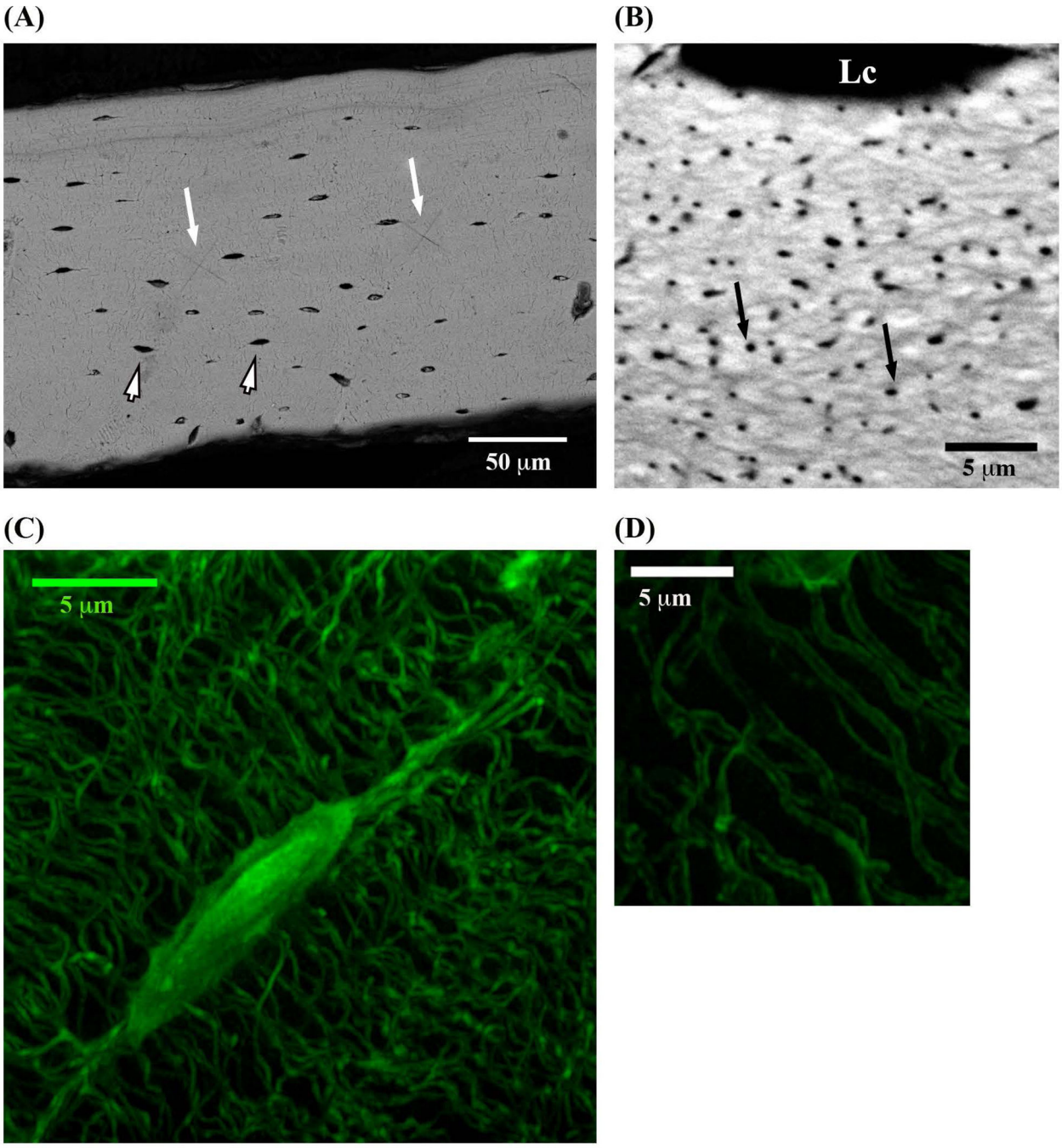

Fig. 2.

(*A*) BSEM image of the anterior mid-diaphysis cortex cross section of mouse femur (small arrowheads indicate osteocyte lacunae, longer white arrows show residual indents from mechanical testing). (*B*) BSEM image of longitudinal section through anterior femoral cortex, showing large numbers of canaliculi in cross-sectional view (black arrows) as well as an osteocyte lacuna (Lc) at the top of the image. (*C*) 3D Z-stack SIM image of osteocyte lacuna and canaliculi and (*D*) SIM visualization of canalicular lumena. Lc = lacuna.

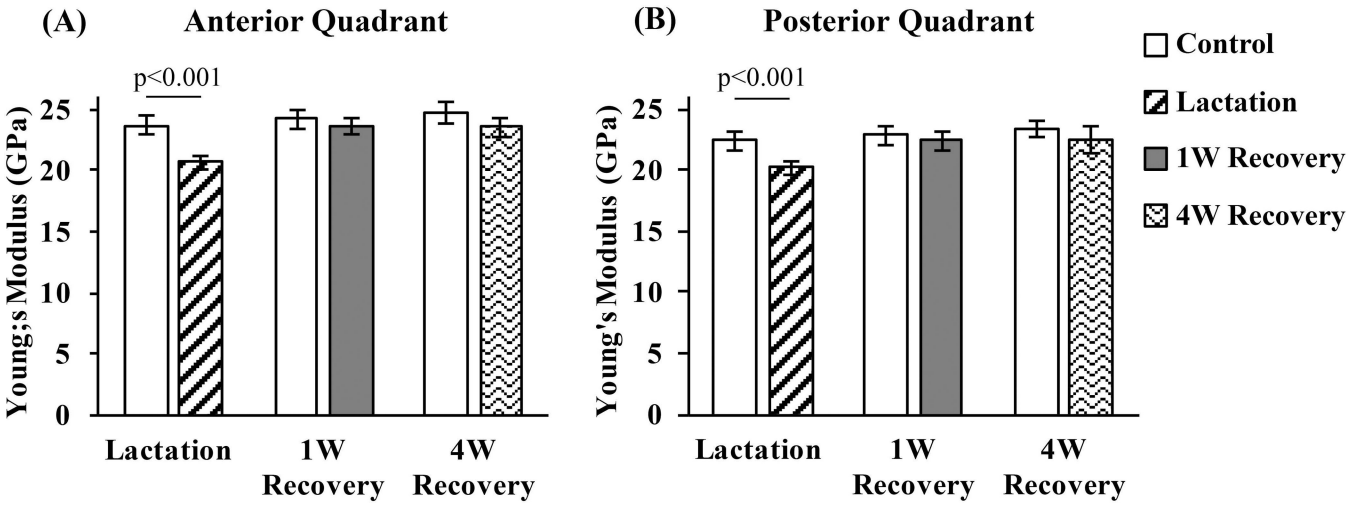

Fig. 3.

Elastic moduli (GPa) in the anterior (*A*) and posterior (*B*) mid-diaphyseal cortex of mouse femur following lactation and recovery, measure from microindentation testing. ($p < 0.001$ versus age-matched control bone).

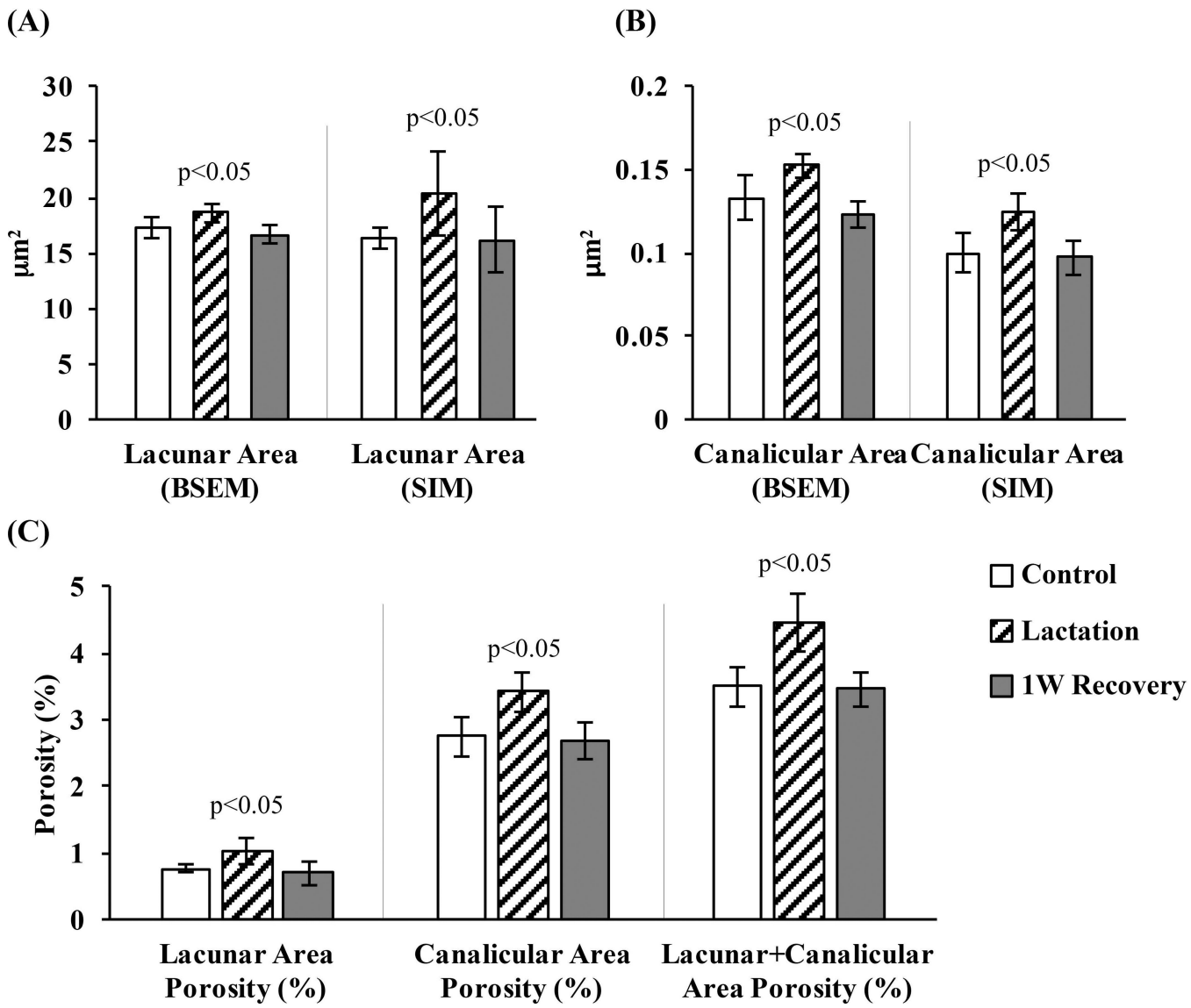

Fig. 4.

(*A*) Lacunar and (*B*) canalicular area (μm^2) for control, lactation and 1-week recovery groups, determined using BSEM and SIM images, showing increases in void space with lactation and recovery to baseline within 1-week postlactation. (*C*) Lacunar, canalicular, and combined lacunar+canalicular porosity (BSEM studies) in control, lactation, and 1-week recovery bones, expressed as percentage of bone volume ($p < 0.05$ versus age-matched control).

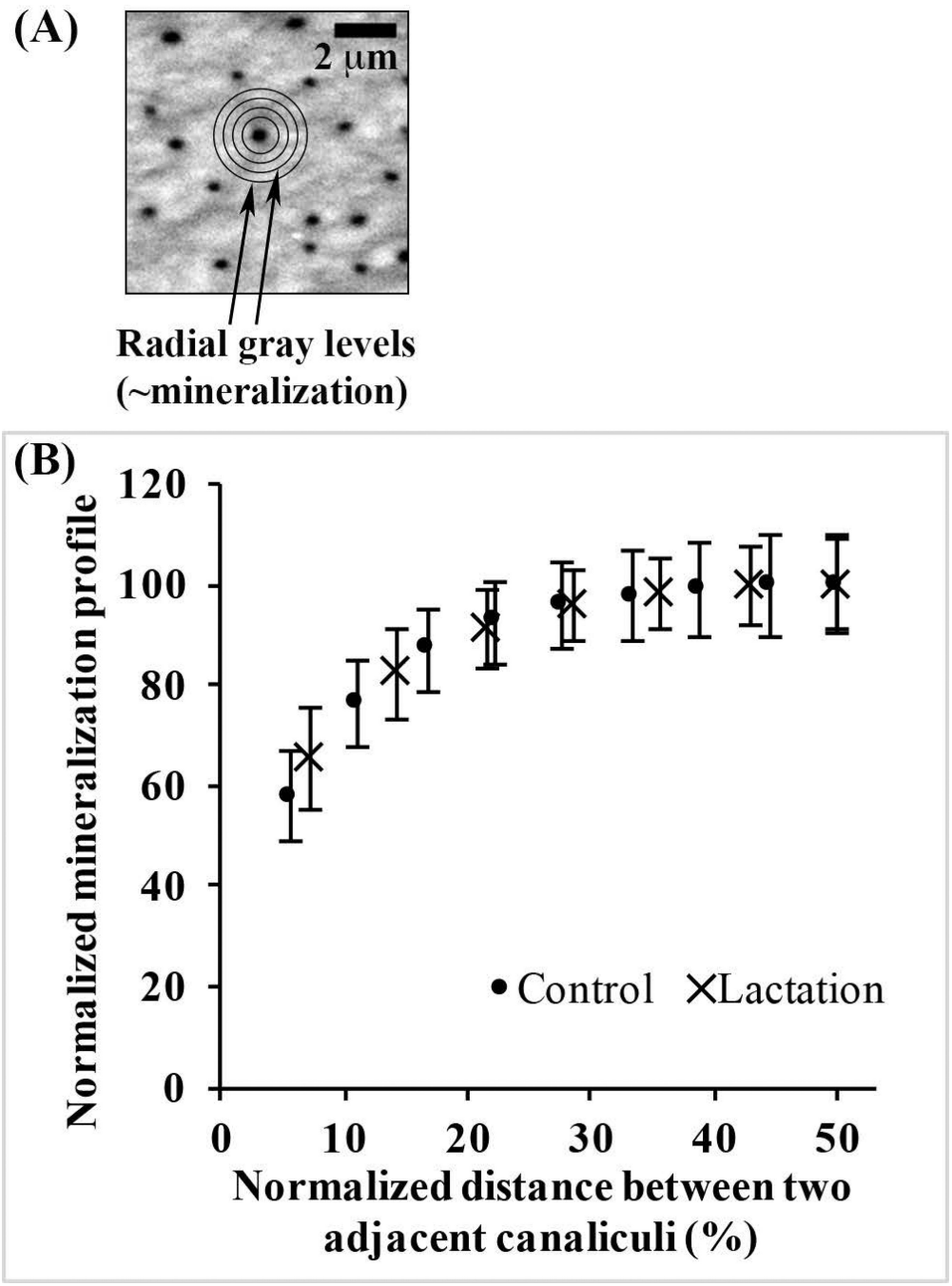

Fig. 5.

(*A*) BSEM image of longitudinal section through a mouse femoral diaphysis, showing canaliculi in cross-section. A single canaliculus with sampling overlay was used for radial distance measurement of mineralization. (*B*) Normalized mineralization plotted versus normalized distance from canalicular walls for control and lactation bones, showing no difference in matrix mineralization distribution profiles between groups. (Note: Offset in distances between treatment groups reflects effect of canalicular enlargement and for

simplicity, data are shown from the canalicular wall to half the distance to adjacent canaliculi, as data beyond the midpoint are the mirror image of those shown).

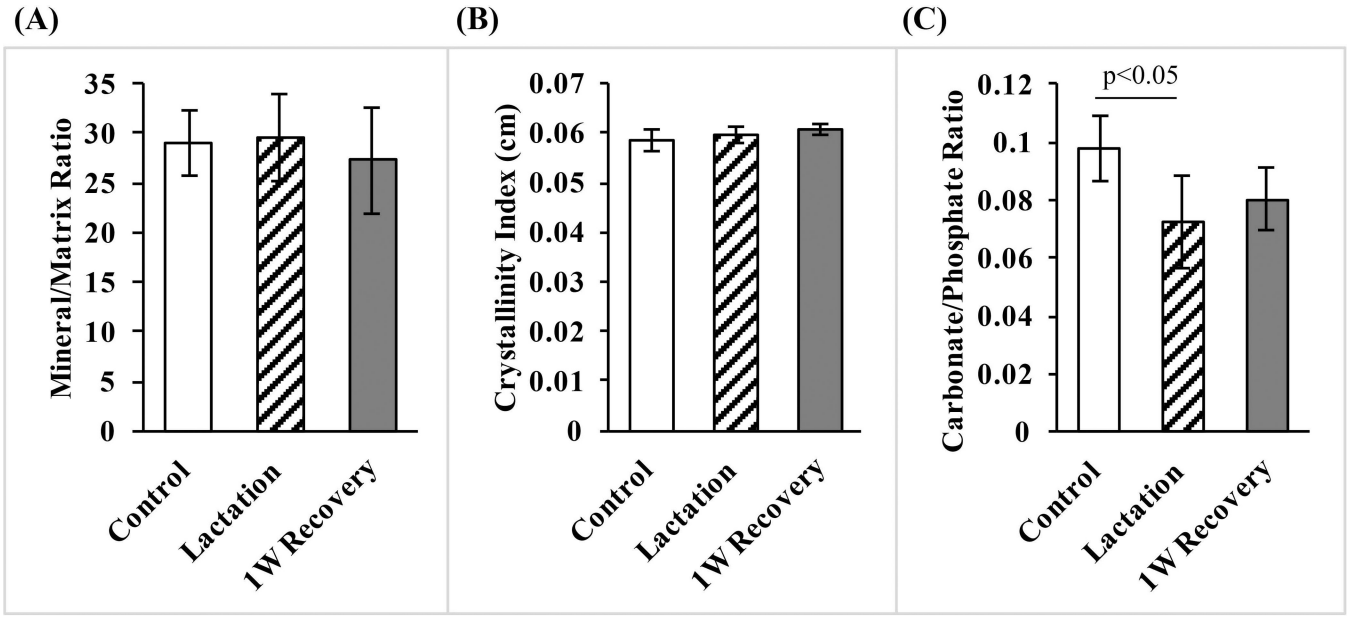

Fig. 6.

(*A*) Mineral/matrix ratio, (*B*) crystallinity, and (*C*) carbonate/phosphate ratio for control, lactation, and 1-week recovery bones obtained by Raman microspectroscopy. Lactation resulted in a significant ($p < 0.05$) carbonate loss that did not recover after cessation of lactation.